Original Research Article

Computer-aided drug design of small-molecule compounds targeting TIM-3 for cancer immunotherapy

Abstract

Aims: To identify potential small-molecule inhibitors of TIM-3 through computational approaches and evaluate their interactions, stability, and structural dynamics.

Study Design: A computational drug discovery study utilizing virtual screening, molecular docking, and molecular dynamics simulations.

Place and Duration of Study: Conducted at the Department of Chemistry and Chemical Engineering, University of New Haven, USA, from January to December 2024.

Methodology: A pharmacophore/similarity search was conducted using the PUBCHEM database, followed by molecular docking simulations to identify compounds with favorable binding properties to TIM-3. Three top-performing compounds (CID_146311758-TIM3, CID_164628526_TIM-3, and CID_146301996-TIM3) were analyzed further using molecular dynamics simulations to assess their binding stability, structural compactness, and hydrogen bond interactions.

Results: CID_164628526_TIM-3 displayed stable binding, minimal fluctuations, and a compact structure closely resembling the reference compound YQG. CID_146311758-TIM3 and CID_146301996-TIM3 showed higher flexibility and fluctuations. Hydrogen bond analysis indicated that CID_164628526_TIM-3 formed fewer bonds on average. These findings suggest that CID_164628526_TIM-3 is a promising candidate for further investigation.

Conclusion: This study highlights the potential of computational approaches to identify small-molecule inhibitors for TIM-3. CID_164628526_TIM-3 emerges as a promising candidate, providing a foundation for developing novel therapeutic agents targeting TIM-3 to enhance immune responses against tumors.

UNDER PEER REVIEW

Keywords: Computer-aided drug design, TIM-3, Cancer immunotherapy, Molecular docking, Molecular dynamics simulation.

1.0 Introduction

Over the course of the past decade, there has been a remarkable transformation in the field of cancer treatment as immunotherapy has emerged as a groundbreaking approach (Baxevanis et al., 2009; Morrison et al., 2018). By harnessing the remarkable capabilities of the immune system to target and eliminate cancer cells, immunotherapy offers a highly promising pathway towards long-lasting and potentially curative responses across a wide range of cancer types (Abbott and Ustoyev, 2019). Central to the success of immunotherapy is the regulation of T-cell activation and effector functions, which rely on a delicate balance of co-stimulatory and co-inhibitory signals (Yu et al., 2019). Among these regulatory factors, immune checkpoints such as programmed cell death protein 1 (PD-1), cytotoxic T-lymphocyte-associated antigen 4 (CTLA-4), and T-cell immunoglobulin and mucin-domain containing-3 (TIM-3) play critical roles in preserving immune homeostasis and preventing autoimmunity (Abbott and Ustoyev, 2019; Yu et al., 2019).

TIM-3, a transmembrane protein expressed on select immune cells, has emerged as a pivotal immune checkpoint receptor in the realm of cancer immunology. Initially identified as a negative regulator of immune responses, particularly those of the Th1 type, TIM-3 has now been recognized for its involvement in tumor immunity and the establishment of immunosuppressive environments (O'Donnell et al., 2019). The presence of TIM-3 extends beyond a single immune cell type, with its expression observed on various key players such as CD4+ and CD8+ T-cells, regulatory T-cells (Tregs), natural killer (NK) cells, dendritic cells (DCs), and myeloid-derived suppressor cells (MDSCs) (Saleh and Elkord, 2020). Notably, within the tumor microenvironment, TIM-3 expression is heightened, suggesting its significant role in driving tumor-induced immune dysfunction. Activation of TIM-3 entails a complex series of interactions with its ligands, predominantly galectin-9 (Gal-9), phosphatidylserine (PtdSer), and

UNDER PEER REVIEW

carcinoembryonic antigen-related cell adhesion molecule 1 (CEACAM1) (Zhang et al., 2016). This activation cascade leads to the recruitment of downstream signaling molecules, including Src homology 2 domain-containing protein tyrosine phosphatase-1 (SHP-1) and Bat3, culminating in the suppression of T-cell function. Evidence is mounting to suggest cross-talk between TIM-3 and other immune checkpoints, such as PD-1, CTLA-4, lymphocyte activation gene 3 (LAG-3), and T-cell immunoreceptor with Ig and ITIM domains (TIGIT) (Shi et al., 2021). These interactions underscore the complexity of immune checkpoint regulation and open up avenues for potential synergistic targeting approaches. The presence of elevated TIM-3 expression within tumor-infiltrating lymphocytes (TILs) has been correlated with unfavorable prognoses across multiple cancer types (Vlaming et al., 2022). Such high TIM-3 expression has been linked to more aggressive tumor characteristics, increased propensity for metastasis, and diminished overall survival rates, thereby highlighting its potential as a valuable prognostic biomarker (Qin et al., 2020). Additionally, TIM-3 expression has been put forward as a promising predictive biomarker for assessing immunotherapy response. Studies have demonstrated that tumors exhibiting heightened levels of TIM-3 expression tend to be less responsive to immune checkpoint blockade, suggesting the potential utility of TIM-3 in tailoring treatment strategies to individual patients (Das et al., 2017; Qin et al., 2020). Given the escalating importance of TIM-3 as a biomarker, ongoing efforts are dedicated to the development of robust and standardized techniques for detecting TIM-3.

The therapeutic blockade of TIM-3 utilizing antibodies has exhibited noteworthy achievements in the treatment of various human malignancies, and ongoing clinical trials further substantiate its potential (Acharya et al., 2020; Liikanen et al., 2022). It has been reported that the primary mode of action for anti-TIM-3 antibodies lies in their ability to impede the interaction between TIM-3 and PtdSer as well as CEACAM1 (Sebatos-Peyton et al., 2017). However, one limitation associated with antibodies is their relatively limited capacity to penetrate tumors effectively (Thurber et al., 2008). As a result, substantial efforts have been dedicated to the development of small molecule inhibitors targeting TIM-3 (Wu et al., 2023).

To date, only a single peptide and a solitary small molecule inhibitor have been reported as viable options in targeting TIM-3 (Wu et al., 2023). The small molecule inhibitor known as CA-327 demonstrates the unique capability of targeting both TIM-3 and PD-L1, thereby exhibiting a

UNDER PEER REVIEW

certain degree of anti-tumor efficacy (Wu et al., 2023). Nonetheless, the structural details of CA-327 have not been publicly disclosed, and a comprehensive understanding of the precise mechanisms through which it exerts its anti-tumor activity remains incomplete (Testa et al., 2020). Consequently, the exploration and identification of novel small molecule inhibitors that specifically target TIM-3 assume utmost significance in the realm of cancer treatment.

The quest for novel small molecule inhibitors represents a critical step forward in combating cancer by effectively targeting TIM-3. By expanding our arsenal of therapeutic options, we can potentially overcome the limitations associated with antibody-based treatments and advance towards more tailored and efficacious approaches for TIM-3 blockade (Wu et al., 2023).

In this study, the aim of our research is to investigate the therapeutic potential of targeting TIM-3 in cancer treatment. By employing computational chemistry and drug discovery approaches, our goal is to identify novel small molecule inhibitors that can effectively bind to TIM-3, modulate its activity, and disrupt the immunosuppressive tumor microenvironment. As a starting point for our virtual screening campaign, we performed a pharmacophore/similarity search utilizing the PUBCHEM database to identify compounds similar to YQG, a co-crystal inhibitor of TIM-3. Next, to prioritize and select compounds with favorable binding energies and key molecular interactions, we conduct molecular docking simulations to explore the binding interactions between the identified compounds and the active site of TIM-3. Finally, molecular dynamics simulationswas performed to investigate the conformational dynamics, stability, and intermolecular interactions of the selected compounds with TIM-3 over an extended period of time.

2.0 Materials and Methods

2.1 Pharmacophore/Similarity Search

For the purpose of identifying compounds that bear resemblance to YQG, which happens to be a co-crystal inhibitor of TIM-3 (Rietz et al., 2021), we carefully conducted a pharmacophore/similarity search employing the vast resources of the PUBCHEM database (Kim et al., 2021). This particular approach entailed scrutinizing an extensive collection of compounds in order to uncover those possessing comparable chemical attributes and structural traits akin to

UNDER PEER REVIEW

YQG. From this comprehensive search, we curated a subset of 143 compounds, which were subsequently earmarked for subsequent in-depth analysis and investigation.

2.2 Structure-based Virtual screening

We used the cutting-edge Autodock Vina program, which is renowned for its ability in this domain, to carry out the careful docking simulation (Trott and Olson, 2010). The protein structure of TIM-3, which served as the main component of our study, was sourced from the renowned Protein Data Bank (PDB) under the unique identification 7m41 (Rietz et al., 2021). By carefully identifying and defining the protein's active site, we focused our attention on a set of residues, including Asp53, Val54, Trp57, Ser59, Arg60, Tyr61, Trp62, Phe67, and Arg68, which together form TIM-3's main pocket (Rietz et al., 2021). Careful attention was paid to defining the size of the grid box in order to precisely map the spatial properties of the protein active site. This grid box's dimensions were specified with exactitude to be 60 units along the x-axis, 50 units along the y-axis, and 40 units along the z-axis. This grid box's center was carefully determined to be at (-19.079, -37.352, 5.951), which pinpointed the focus of our docking exploration. In order to achieve the accurate modeling of the intermolecular interactions within this simulated environment, a spacing of 0.375 angstroms was purposefully chosen. Our work moved on to the important phase of docking simulations once the active region of TIM-3 was clearly identified. The findings of the prior pharmacophore search yielded 143 compounds, which were carefully chosen and then subjected to this comprehensive computational analysis.By carefully examining the interactions and probable binding mechanisms between these substances and the targeted active site of TIM-3, we were able to get crucial knowledge about prospective inhibitory candidates deserving of further study.

2.3 Molecular Dynamics Simulation

The comprehensive exploration of our research involved not only the pharmacophore/similarity search and docking simulations but also encompassed the pivotal step of conducting molecular dynamics (MD) simulations utilizing the cutting-edge GROMACS 2022.3 software (Van Der Spoel et al., 2005). Our focus was specifically directed towards four complexes of immense interest: CID_146311758-TIM3, CID_164628526_TIM-3, CID_146301996-TIM3, and YQG-TIM3. To ensure the accurate representation of the intricate interplay between ligands and the protein, we employed the CHARMM36 force field to effectively parameterize both components

UNDER PEER REVIEW

within the system (Vanommeslaeghe et al., 2010). By carefully accounting for the diverse molecular properties, we established a foundation for a rigorous investigation into the conformational dynamics and stability of the ligand-protein interactions.

The solvation step involved surrounding the complexes under investigation, namely CID_146311758-TIM3, CID_164628526_TIM3, CID_146301996-TIM3, and YQG-TIM3, with an appropriate solvent environment. This solvent, typically water, was carefully chosen to mimic the physiological conditions relevant to the study. By solvating the system, we created a realistic environment that allowed for the accurate representation of the interactions between the compounds and the surrounding solvent molecules. Following solvation, the system underwent an ionization step. Here, appropriate ions (2 sodium ions) were added to maintain the overall system neutrality and to simulate the desired ionic strength. This step ensured the preservation of electrostatic balance within the system, crucial for simulating realistic physiological conditions. Next, the system underwent a minimization process of 5000 nsteps, where steepest descent energy optimization algorithms were employed to relax the initial structure and eliminate any steric clashes or unfavorable interactions. This step involved iteratively adjusting the positions of atoms to reach a more stable energy state, ensuring a starting point for the subsequent MD simulations that was free from significant structural distortions or artifacts. After minimization, the equilibration step was performed to gradually adjust the system from the minimized state to the desired simulation conditions. This involved allowing the system to reach equilibrium by controlling parameters such as temperatureand pressure. The temperature coupling (tcoupl) and pressure coupling (pcoupl) were set as V-rescale and Berendsen respectively. During this process, the system was subjected to a series of restrained or constrained dynamics, gradually releasing these restraints to allow for more freedom of motion and achieving a stable equilibrium state. These steps—solvation, ionization, minimization, and equilibration—were integral in setting up the system for the subsequent MD simulations. By meticulously following these protocol steps, we ensured that the system was well-prepared, stable, and representative of the physiological conditions of interest. The MD simulations were then conducted over a production run spanning a duration of 100 nanoseconds (ns) for each of the aforementioned complexes. This extended timescale allowed us to explore and elucidate the subtle nuances of the ligand-protein interactions, shedding light on their binding modes, calculating binding energies, and carefully

UNDER PEER REVIEW

monitoring the structural stability and dynamics of these complexes throughout the simulation trajectories.

3.0 Results and Discussion

3.1 Molecular docking-based virtual screening

In our docking-based virtual screening method, we initiated the process by conducting a redocking experiment. The goal was to assess the accuracy and reliability of our docking protocol by comparing the binding mode of the redocked YQG compound with the experimentally determined co-crystal pose of YQG (Rietz et al., 2021). Encouragingly, our redocking results indicated a close resemblance between the binding modes of the redocked YQG compound and the reference co-crystal structure, thereby validating the efficacy of our docking protocol (Figure 1) (Adelusi et al., 2021). Building upon this validation, we proceeded with docking simulations involving 143 pharmacophores derived from the YQG compound. Our aim was to identify potential compounds that exhibit superior binding energy in comparison to the reference molecule, YQG, which possessed a binding energy of -8.3 kcal/mol (Figure 2). The docking results unveiled three noteworthy compounds, namely CID_146311758-TIM3, CID_164628526_TIM-3, and CID_146301996-TIM3, all of which demonstrated more favorable binding energies (-8.6 kcal/mol, -8.6 kcal/mol, and -8.4 kcal/mol, respectively) when compared to YQG (Figure 2, Supplementary Table 1). Further analysis of the binding interactions shed light on the intricate molecular associations between these compounds and the active pocket of TIM3 (Rietz et al., 2021). CID_146311758-TIM3 was found to engage in four hydrogen bonds with key residues, namely Asp53, Arg60, and Arg68 (Figure 3). Additionally, pi-pi stacking interactions were observed with Trp57 and Trp62, along with pi-sigma bonding with Val54, pi-sulfur interaction with Phe67, and a carbon-hydrogen bond involving Ser59. As for CID_164628526_TIM-3, its binding interaction profile included pi-pi stacking with Trp57 and Trp62, pi-alkyl bonding with Val54 and Phe67, and a pi-pi T-shaped interaction with Phe67 (Figure 3). Lastly, CID_146301996-TIM3 demonstrated four hydrogen bond interactions with Asp53, Arg60, and Arg68, although an unfavorable hydrogen bond was observed with Tyr61 (Figure 3). Additionally, pi-sulfur bonding with Phe67, pi-sigma interaction with Val54, pi-pi stacking interactions with Trp57 and Trp62, and a carbon-hydrogen bond with Ser59 contributed

UNDER PEER REVIEW

to its binding pattern. Overall, these interactions firmly establish the binding of the four identified compounds to the active pocket of TIM3 protein. Consequently, they hold considerable promise as potential drug candidates for the treatment of TIM3-associated cancer patients. The comprehensive molecular docking analysis, encompassing the validation of our docking protocol, the identification of superior binding energies, and the detailed characterization of key binding interactions, contributes to our understanding of the molecular mechanisms underlying the interactions between these compounds and TIM3.

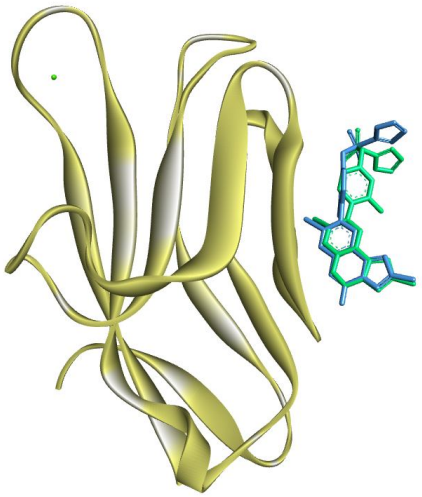

Figure 1: Superimposition of the redocked X-ray structure of YQG (green) with the experimental pose (blue).

UNDER PEER REVIEW

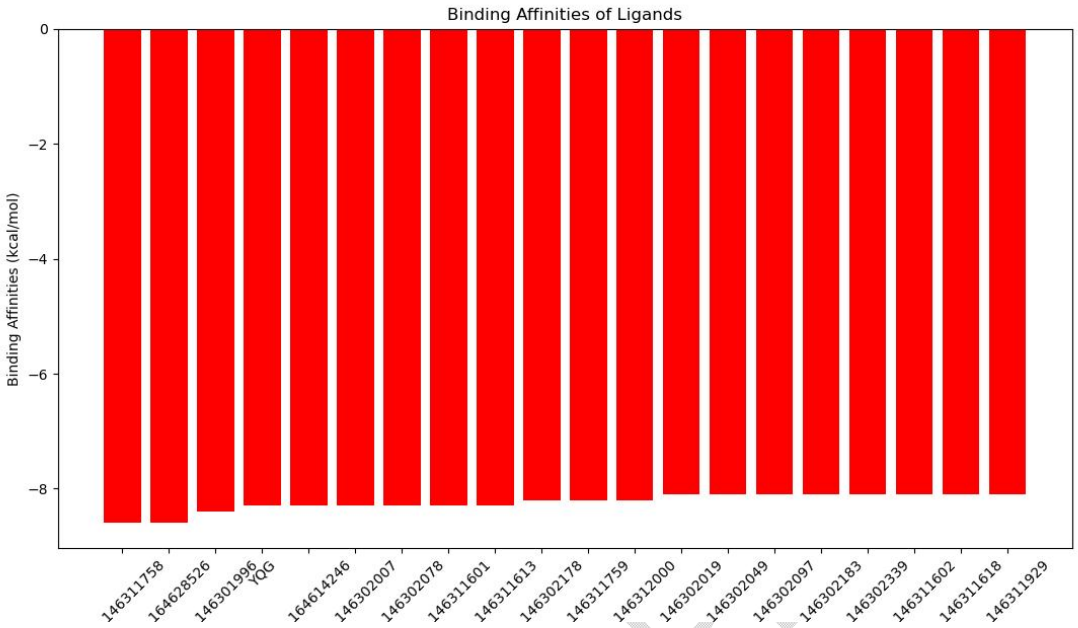

Figure 2: Top 20 scoring compounds from the Docking-based virtual screening.

CID_164628526-TIM3	CID_164628526-TIM3
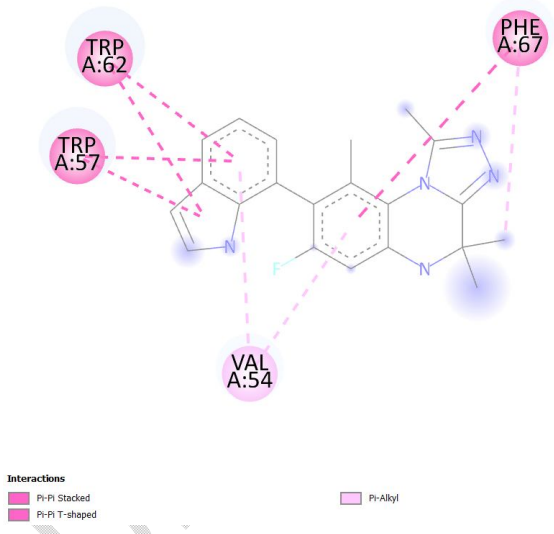	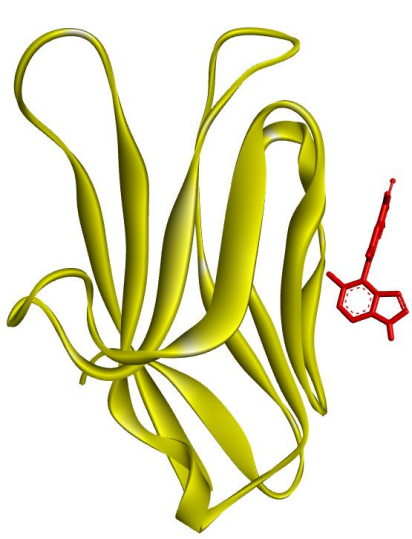
CID_146311758-TIM3	CID_146311758-TIM3

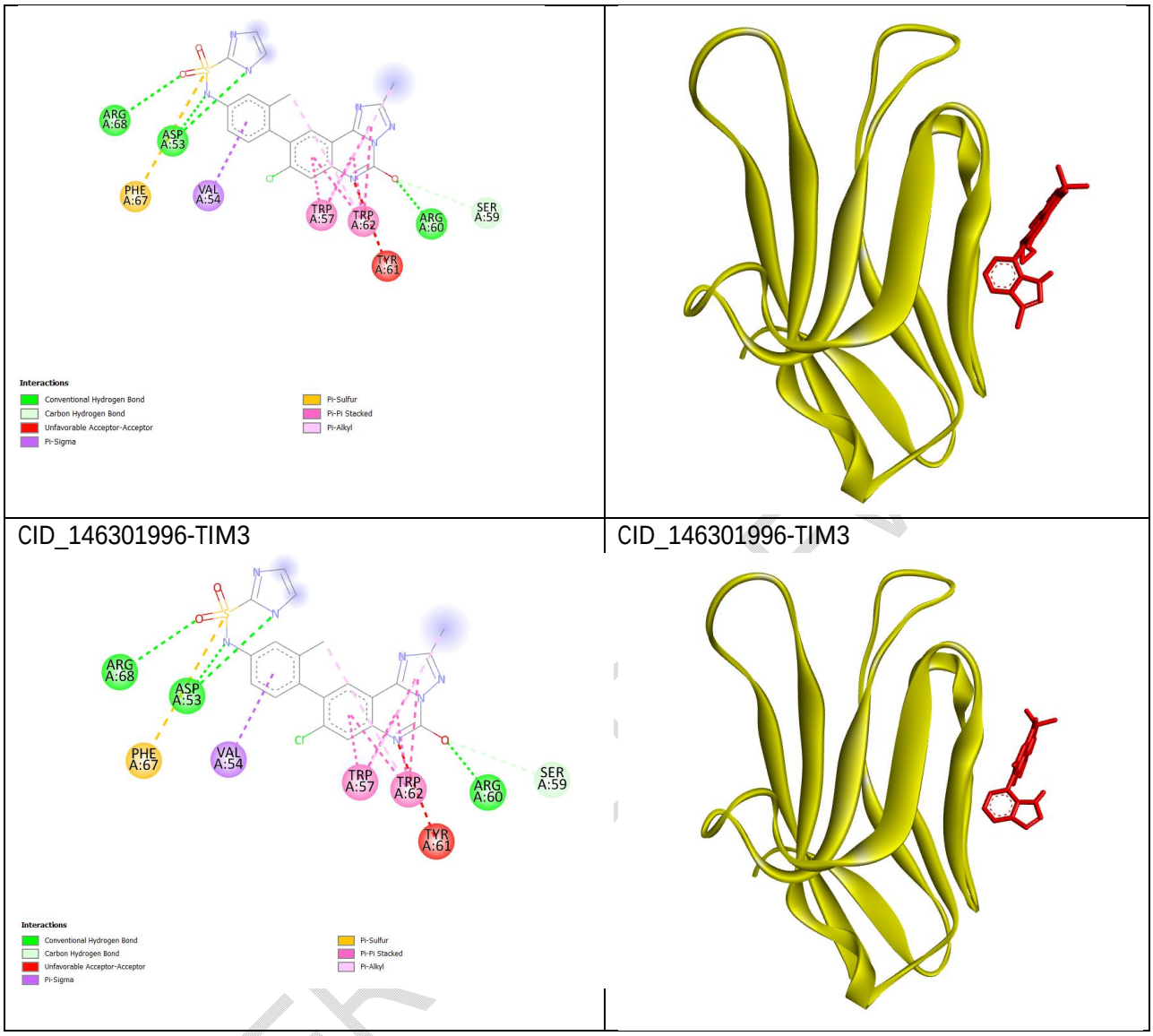

Figure 3: The 2D (Left) and 3D (Right) structures of the Top3 hit candidates in complex with the TIM3 receptor.

3.2 Molecular dynamics simulation

3.2.1 RMSD analysis

During the molecular dynamics simulation, the Root Mean Square Deviation (RMSD) was calculated to assess the stability and structural changes of the complexes (Ogunlana et al., 2022). The average RMSD values for the different complexes are as follows: CID_146311758-TIM3 averaged 0.55 nm, CID_164628526_TIM-3 averaged 0.30 nm, CID_146301996-TIM3 averaged 0.46 nm, and YQG-TIM3 averaged 0.23 nm (Table 1). The RMSD values provide insights into

the deviation of each complex's structure from the starting conformation (Adelusi et al., 2022). By analyzing the spectrum of each complex, it is evident that CID_164628526_TIM-3 exhibits minimal fluctuation throughout the entire simulation period and closely resembles the standard (YQG) in terms of the average RMSD (Figure 4). This indicates that CID_164628526_TIM-3 maintains a stable structure with relatively minor changes over time. In contrast, CID_146311758-TIM3 and CID_146301996-TIM3 do not maintain a consistently stable RMSD spectrum throughout the entire simulation (Figure 4). CID_146311758-TIM3 shows maximal or abrupt fluctuation between 38 ns and 95 ns before the spectrum sharply decreases around 97 ns. Subsequently, it maintains minimal fluctuation until the end of the simulation. Similarly, CID_146301996-TIM3 exhibits abrupt fluctuation starting around 50 ns, which continues throughout the entire 100 ns simulation period. This suggests that CID_146301996-TIM3 undergoes more substantial structural changes and displays greater flexibility compared to the other complexes. The observed fluctuations in RMSD indicate variations in the conformations and structural integrity of the complexes over time (Oyedele et al., 2022). These findings highlight the importance of considering the stability and structural dynamics of the compounds when assessing their potential as drug candidates.

Table 1: The statistical average mean values of the RMSD, RMSF, ROG and H-bond of the compounds (including the Standard) in complex with TIM3.

Complexes	Average RMSD (nm)	Average RMSF (nm)	Average ROG (nm)	Average H-bond (nm)
CID_164628526_TIM-3	0.30	0.14	1.39	0.58
CID_146311758-TIM3	0.55	0.21	1.46	0.77
CID_146301996-TIM3	0.46	0.18	1.42	0.20
YQG-TIM3	0.23	0.14	1.38	2.28

UNDER PEER REVIEW

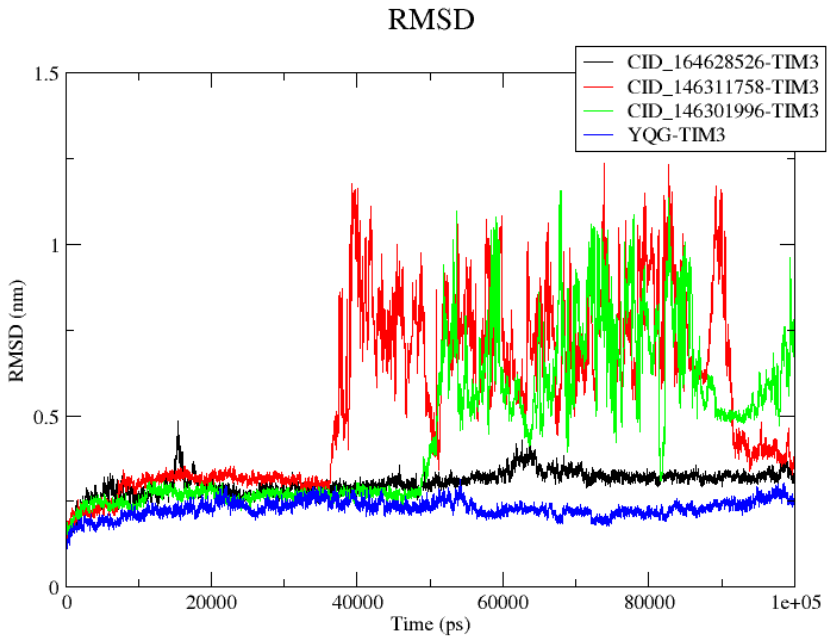

Figure 4: The RMSD spectrum of the top scoring compounds and YQG in complex with TIM3.

3.2.2 RMSF analysis

The Root Mean Square Fluctuation (RMSF) analysis provides insights into the flexibility and dynamic behavior of the complexes during the molecular dynamics simulation. By calculating the average RMSF values for each complex, we can assess the extent of atomic fluctuations within the protein structure (Ogunlana et al., 2023). The average RMSF values for CID_164628526_TIM3, CID_146311758-TIM3, CID_146301996-TIM3, and YQG-TIM3 are 0.14 nm, 0.21 nm, 0.18 nm, and 0.14 nm, respectively (Table 1). Interestingly, both CID_164628526_TIM-3 and YQG-TIM3 display the same average RMSF value of 0.14 nm. This suggests that these two complexes exhibit similar levels of atomic fluctuations within their respective protein structures (Figure 5). The consistency between the RMSF and RMSD results further supports the notion that CID_164628526_TIM-3 is a promising hit candidate. The lower average RMSF value indicates that this compound experiences relatively less fluctuation and maintains a more stable protein structure during the simulation (Adelusi et al., 2022). This finding aligns with the observation from the RMSD analysis, where CID_164628526_TIM-3

UNDER PEER REVIEW

demonstrated minimal fluctuation and closely resembled the standard YQG-TIM3. Comparatively, CID_146311758-TIM3 and CID_146301996-TIM3 display higher average RMSF values of 0.21 nm and 0.18 nm, respectively (Table 1). These complexes exhibit relatively more atomic fluctuations, suggesting increased flexibility within their protein structures. The consistency between the RMSF and RMSD results reinforces the potential of CID_164628526_TIM-3 as a promising hit candidate. Its stable structure, combined with minimal fluctuations and low RMSD values, indicates a higher degree of conformational stability and structural integrity (Oyedele et al., 2023). By considering both the RMSF and RMSD analyses, we can confidently conclude that CID_164628526_TIM-3 stands out as the most promising hit candidate. Its stable structure, minimal fluctuations from RMSF and RMSD values make it a strong contender for further investigation and potential therapeutic applications.

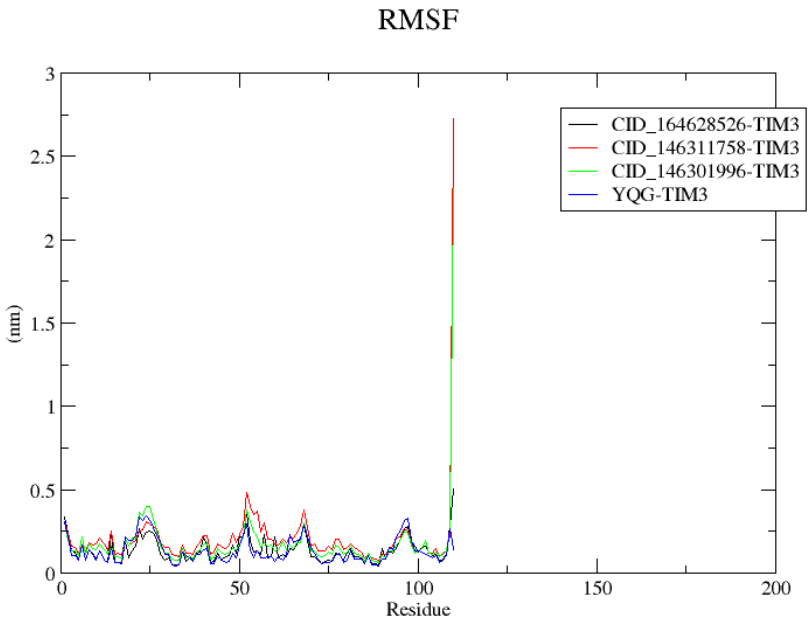

Figure 5: The RMSF spectrum of the top scoring compounds and YQG in complex with TIM3.

3.2.3 ROG

The Radius of Gyration (ROG) analysis provides valuable insights into the compactness and overall size of the protein structures within the complexes (Adelusi et al., 2022). By examining the average ROG values for each complex, we can assess their relative compactness and compare them to the reference YQG-TIM3. The average ROG values for CID_164628526_TIM-3, CID_146311758-TIM3, and CID_146301996-TIM3 are 1.39 nm, 1.46 nm, and 1.42 nm, respectively (Table 1). Comparing these values to the reference YQG-TIM3, which has an average ROG value of 1.38 nm, we can observe that all the complexes exhibit similar levels of compactness, as their ROG values are in close proximity. Again, the ROG results align with the findings from the RMSD and RMSF analyses, further reinforcing the reliability and consistency of our observations. The lower ROG value for CID_164628526_TIM3, the most promising hit candidate, indicates a slightly more compact structure compared to the other complexes. This suggests that CID_164628526_TIM3 may have a more stable and tightly folded protein conformation, potentially enhancing its binding affinity and stability within the active site of TIM-3 (Oyedele et al., 2022).

In addition to the average ROG values, it is important to consider the ROG spectrum and fluctuations exhibited by each complex during the simulation. By examining the ROG spectra, we can gain insights into the dynamic behavior and changes in the compactness of the protein structures over time (Adelusi et al., 2022). Upon analyzing the ROG spectra, it becomes evident that CID_164628526_TIM-3 and YQG-TIM3 exhibit remarkably similar patterns throughout the entire simulation period (Figure 6). This similarity suggests that these two complexes maintain consistent levels of compactness, indicating a relatively stable conformation and limited structural fluctuations. In contrast, CID_146311758-TIM3 and CID_146301996-TIM3 display more pronounced ROG fluctuations (Figure 6). After approximately 39 ns, CID_146311758-TIM3 shows a notable increase in ROG values, indicating a temporary expansion or alteration in its protein structure. Similarly, CID_146301996-TIM3 exhibits a significant increase in ROG values starting around 50 ns, suggesting a distinct change in its compactness. However, both complexes experience a subsequent decrease in ROG values around 90 ns, indicating a return to a more compact conformation. These observations parallel the findings from the RMSD analysis, where CID_146311758-TIM3 and CID_146301996-TIM3 demonstrated maximal fluctuations within their structures. The agreement between the ROG and RMSD results reinforces the consistency and reliability of our findings. Furthermore, the comparison of ROG values among

UNDER PEER REVIEW

the complexes highlights the superior performance of CID_164628526_TIM-3. Its lower average ROG value, coupled with minimal fluctuations and closer resemblance to the reference YQG-TIM3, suggests a more stable and compact protein structure throughout the simulation (Boyenle et al., 2022). This stability may contribute to the potential of CID_164628526_TIM-3 as a promising hit candidate for further investigation and potential therapeutic development. By considering both the average ROG values and the dynamic ROG spectra, we gain a comprehensive understanding of the structural changes and compactness variations exhibited by the complexes. These insights further support the selection and prioritization of CID_164628526_TIM-3 as a top candidate for future studies and highlight its potential for modulating the activity of TIM-3 in cancer treatment.

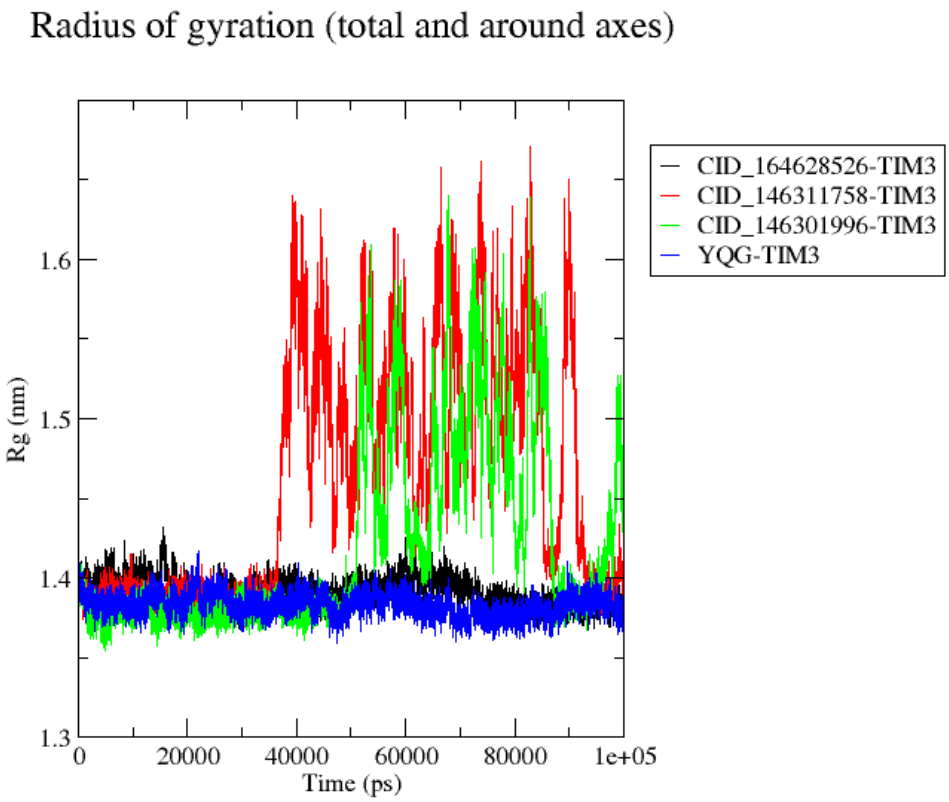

Figure 6: The ROG spectrum of the top scoring compounds and YQG in complex with TIM3.

3.2.4 Intermolecular H-bond

The analysis of intermolecular hydrogen bonds could provide valuable insights into the strength and frequency of these interactions between the ligands and the TIM-3 protein. By examining the average number of H-bonds formed by each complex, we can assess their potential for stable and specific binding interactions (Ayoub et al., 2014). The average number of H-bonds for CID_164628526_TIM-3, CID_146311758-TIM3, and CID_146301996-TIM3 were found to be 0.58, 0.77, and 0.20, respectively (Table 1 and Figure 7). In comparison, YQG-TIM3 exhibited an average of 2.28 H-bonds. The results indicate varying degrees of H-bond formation among the complexes. CID_164628526_TIM-3 displayed the lowest average number of H-bonds, indicating a relatively weaker tendency for H-bond formation with the TIM-3 protein. On the other hand, CID_146311758-TIM3 had a slightly higher average number of H-bonds, suggesting a stronger potential for H-bond interactions (Figure 7). Interestingly, CID_146301996-TIM3 showed the lowest average number of H-bonds among the three compounds, indicating a relatively weaker propensity for H-bond formation with TIM-3 (Adelusi et al., 2022). This observation suggests that CID_146301996-TIM3 may rely on other types of interactions, such as hydrophobic interactions or electrostatic forces, for binding to the target protein. In contrast, YQG-TIM3 exhibited the highest average number of H-bonds, indicating a stronger capability to form these specific interactions with the TIM-3 protein. This finding is consistent with YQG being a known co-crystal inhibitor of TIM-3 and supports its role as a reference compound in our study (Rietz et al., 2021). The variation in H-bonding observed among the compounds underscores the importance of analyzing different molecular interactions in drug discovery. While H-bonding is often considered a crucial determinant of ligand-protein binding affinity, other factors such as hydrophobic interactions, electrostatic forces, and steric effects also contribute to the overall stability and efficacy of the interactions. Overall, the intermolecular H-bond analysis provides valuable information about the strength and nature of the interactions between the compounds and the TIM-3 protein (Adelusi et al., 2022).

UNDER PEER REVIEW

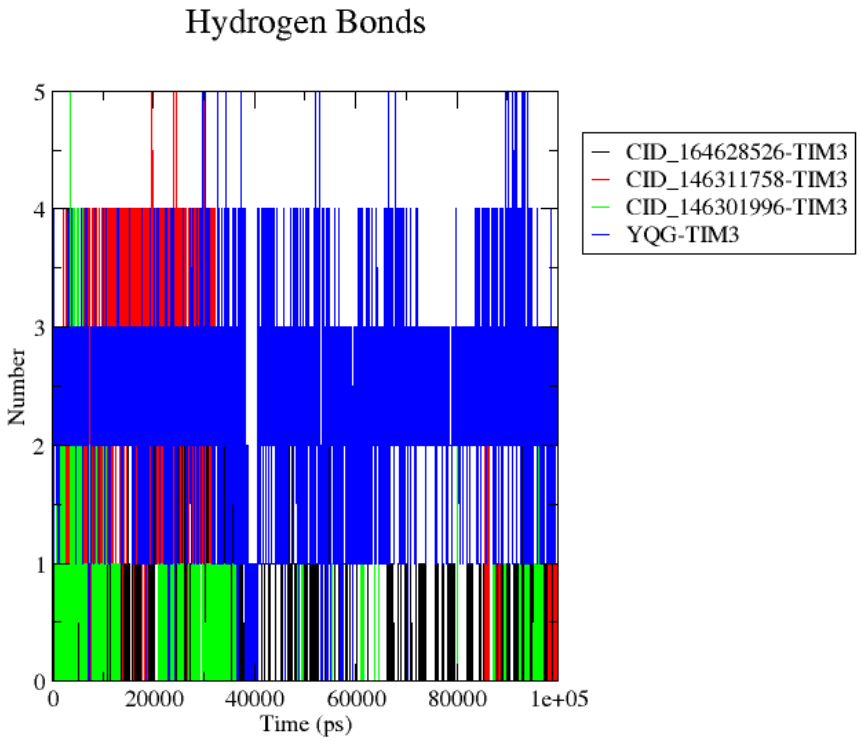

Figure 7: The Intermolecular H-bond spectrum of the top scoring compounds and YQG in complex with TIM3.

UNDER PEER REVIEW

Conclusion

In recent years, TIM-3 has emerged as a promising target for cancer immunotherapy due to its involvement in tumor immune evasion and suppression. Dysregulated TIM-3 signaling has been associated with immune dysfunction and tumor progression in multiple cancer types, making it an attractive target for therapeutic intervention. However, despite the potential of TIM-3 as a therapeutic target, the development of effective inhibitors remains a challenge. Traditional drug discovery approaches are often time-consuming and costly, requiring extensive screening of large compound libraries. In this context, computational methods such as molecular docking-based virtual screening and molecular dynamics simulations offer valuable tools for accelerating the identification and optimization of potential drug candidates.

In this study, our molecular docking-based virtual screening and molecular dynamics simulation analyses have provided valuable insights into the potential of compounds for targeting TIM-3 in cancer treatment. The docking results identified three compounds, namely CID_146311758-TIM3, CID_164628526_TIM-3, and CID_146301996-TIM3, which exhibited superior binding energies compared to the reference molecule, YQG. Detailed analysis of the binding interactions revealed the intricate molecular associations between these compounds and the active pocket of TIM-3. The molecular dynamics simulation further assessed the stability and dynamic behavior of the complexes through RMSD, RMSF, and ROG analyses. Among the compounds, CID_164628526_TIM-3 demonstrated minimal fluctuations, low RMSD and RMSF values, and a slightly more compact structure, closely resembling the reference YQG-TIM3. These findings suggest a higher degree of conformational stability and structural integrity for CID_164628526_TIM-3. Additionally, the intermolecular H-bond analysis highlighted varying degrees of H-bond formation among the compounds, with CID_146311758-TIM3 exhibiting the strongest potential for these interactions. Collectively, these results suggest that CID_164628526_TIM-3 is a promising hit candidate for further investigation and potential therapeutic applications. Further optimization and design efforts can leverage the insights gained from this study to develop small molecule inhibitors with enhanced binding affinity and specificity for TIM-3, ultimately benefiting patients with TIM-3-associated cancers.

UNDER PEER REVIEW

Clinical trial number

Not applicable.

References

1. Abbott M, Ustoyev Y. Cancer and the Immune System: The History and Background of Immunotherapy. Semin Oncol Nurs. 2019 Oct;35(5):150923. doi: 10.1016/j.soncn.2019.08.002. Epub 2019 Sep 13. PMID: 31526550.

2. Acharya N, Sabatos-Peyton C, Anderson AC. Tim-3 finds its place in the cancer immunotherapy landscape. J Immunother Cancer. 2020 Jun;8(1):e000911. doi: 10.1136/jitc-2020-000911. PMID: 32601081; PMCID: PMC7326247.
3. Adelusi TI, Abdul-Hammed M, Idris MO, Kehinde OQ, Boyenle ID, Divine UC, Adedotun IO, Folorunsho AA, Kolawole OE. Exploring the inhibitory potentials of *Momordica charantia* bioactive compounds against Keap1-Kelch protein using computational approaches. In Silico Pharmacol. 2021 Jun 25;9(1):39. doi: 10.1007/s40203-021-00100-2. PMID: 34249600; PMCID: PMC8233444.
4. Adelusi TI, Oyedele AK, Boyenle ID, Ogunlana AT, Adeyemi RO, Ukachi CD, Idris MO, Olaoba OT, Adedotun IO, Kolawole OE, Xiaoxing Y, Abdul-Hammed M. Molecular modeling in drug discovery. Informatics in Medicine Unlocked. 2022;29:100880. ISSN 2352-9148. https://doi.org/10.1016/j.imu.2022.100880.
5. Ayoub AT, Craddock TJA, Klobukowski M, Tuszynski J. Analysis of the strength of interfacial hydrogen bonds between tubulin dimers using quantum theory of atoms in molecules. Biophys J. 2014 Aug 5;107(3):740-750. doi: 10.1016/j.bpj.2014.05.047. PMID: 25099813; PMCID: PMC4129478.
6. Baxevanis CN, Perez SA, Papamichail M. Cancer immunotherapy. Crit Rev Clin Lab Sci. 2009;46(4):167-89. doi: 10.1080/10408360902937809. PMID: 19650714.
7. Boyenle ID, Ogunlana AT, Kehinde Oyedele AQ, Olokodana BK, Owolabi N, Salahudeen A, Aderenle OT, Oloyede TO, Adelusi TI. Reinstating apoptosis using putative Bcl-xL natural product inhibitors: Molecular docking and ADMETox profiling investigations. J Taibah Univ Med Sci. 2022 Nov 14;18(3):461-469. doi: 10.1016/j.jtumed.2022.10.014. PMID: 36818176; PMCID: PMC9906007.
8. Das M, Zhu C, Kuchroo VK. Tim-3 and its role in regulating anti-tumor immunity. Immunol Rev. 2017 Mar;276(1):97-111. doi: 10.1111/imr.12520. PMID: 28258697; PMCID: PMC5512889.
9. Kim S, Chen J, Cheng T, Gindulyte A, He J, He S, Li Q, Shoemaker BA, Thiessen PA, Yu B, Zaslavsky L, Zhang J, Bolton EE. PubChem in 2021: new data content and improved web interfaces. Nucleic Acids Res. 2021 Jan 8;49(D1):D1388-D1395. doi: 10.1093/nar/gkaa971. PMID: 33151290; PMCID: PMC7778930.

10. Liikanen I, Basnet S, Quixabeira DCA, Taipale K, Hemminki O, Oksanen M, Kankainen M, Juhila J, Kanerva A, Joensuu T, Tähtinen S, Hemminki A. Oncolytic adenovirus decreases the proportion of TIM-3^+ subset of tumor-infiltrating $CD8^+$ T cells with correlation to improved survival in patients with cancer. J Immunother Cancer. 2022 Feb;10(2):e003490. doi: 10.1136/jitc-2021-003490. PMID: 35193929; PMCID: PMC8867324.
11. Morrison AH, Byrne KT, Vonderheide RH. Immunotherapy and Prevention of Pancreatic Cancer. Trends Cancer. 2018 Jun;4(6):418-428. doi: 10.1016/j.trecan.2018.04.001. Epub 2018 Apr 30. PMID: 29860986; PMCID: PMC6028935.
12. O'Donnell JS, Teng MWL, Smyth MJ. Cancer immunoediting and resistance to T cell-based immunotherapy. Nat Rev Clin Oncol. 2019 Mar;16(3):151-167. doi: 10.1038/s41571-018-0142-8. PMID: 30523282.
13. Ogunlana AT, Boyenle ID, Ojo TO, Quadri BO, Elegbeleye OE, Ogbonna HN, Ayoola SO, Badmus IO, Manica AK, Joshua KI, Onikute OW, Anamelechi JP, Odetunde A, Falusi AG, Oyedele AK. Structure-based computational design of novel covalent binders for the treatment of sickle cell disease. J Mol Graph Model. 2023 Jun 17;124:108549. doi: 10.1016/j.jmgm.2023.108549. Epub ahead of print. PMID: 37339569.
14. Ogunlana AT, Oyedele AK, Boyenle ID, Ayoola SO, Ajibare AC, Adeyemi AO, Jinadu LA, Adenrele OT, Alausa AO, Adelusi TI. "Computer-aided drug design of some KRAS G12C inhibitors: Targeting the covalent and allosteric binding site for cancer therapy." Informatics in Medicine Unlocked. 2022;32:101032. ISSN: 2352-9148. doi: 10.1016/j.imu.2022.101032.
15. Oyedele AK, Ogunlana AT, Boyenle ID, Ibrahim NO, Gbadebo IO, Owolabi NA, Ayoola AM, Francis AC, Eyinade OH, Adelusi TI. Pharmacophoric analogs of sotorasib-entrapped KRAS G12C in its inactive GDP-bound conformation: covalent docking and molecular dynamics investigations. Mol Divers. 2022 Oct 21. doi: 10.1007/s11030-022-10534-1. Epub ahead of print. PMID: 36271195.
16. Oyedele AK, Owolabi NA, Odunitan TT, Ajibare AC, Jimoh RO, Abdul Azeez WO, Bello-Hassan MT, Soares AS, Adekola AT, Abdulkareem TO, Oyelekan SO, Ashiru MA, Gbadebo IO, Olajumoke HE, Boyenle ID, Ogunlana AT. "The discovery of some promising putative binders of KRAS G12D receptor using computer-aided drug

discovery approach." Informatics in Medicine Unlocked. 2023;37:101170. ISSN: 2352-9148. doi: 10.1016/j.imu.2023.101170.

17. Qin S, Dong B, Yi M, Chu Q, Wu K. Prognostic Values of TIM-3 Expression in Patients With Solid Tumors: A Meta-Analysis and Database Evaluation. Front Oncol. 2020 Aug 4;10:1288. doi: 10.3389/fonc.2020.01288. PMID: 32850398; PMCID: PMC7417611.
18. Rietz TA, Teuscher KB, Mills JJ, Gogliotti RD, Lepovitz LT, Scaggs WR, Yoshida K, Luong K, Lee T, Fesik SW. Fragment-Based Discovery of Small Molecules Bound to T-Cell Immunoglobulin and Mucin Domain-Containing Molecule 3 (TIM-3). J Med Chem. 2021 Oct 14;64(19):14757-14772. doi: 10.1021/acs.jmedchem.1c01336. Epub 2021 Oct 1. PMID: 34597046.
19. Sabatos-Peyton CA, Nevin J, Brock A, Venable JD, Tan DJ, Kassam N, Xu F, Taraszka J, Wesemann L, Pertel T, Acharya N, Klapholz M, Etminan Y, Jiang X, Huang YH, Blumberg RS, Kuchroo VK, Anderson AC. Blockade of Tim-3 binding to phosphatidylserine and CEACAM1 is a shared feature of anti-Tim-3 antibodies that have functional efficacy. Oncoimmunology. 2017 Nov 9;7(2):e1385690. doi: 10.1080/2162402X.2017.1385690. PMID: 29308307; PMCID: PMC5749620.
20. Shi X, Li CW, Tan LC, Wen SS, Liao T, Zhang Y, Chen TZ, Ma B, Yu PC, Lu ZW, Qu N, Wang Y, Shi RL, Wang YL, Ji QH, Wei WJ. Immune Co-inhibitory Receptors PD-1, CTLA-4, TIM-3, LAG-3, and TIGIT in Medullary Thyroid Cancers: A Large Cohort Study. J Clin Endocrinol Metab. 2021 Jan 1;106(1):120-132. doi: 10.1210/clinem/dgaa701. PMID: 33000173.
21. Testa U, Castelli G, Pelosi E. Breast Cancer: A Molecularly Heterogenous Disease Needing Subtype-Specific Treatments. Med Sci (Basel). 2020 Mar 23;8(1):18. doi: 10.3390/medsci8010018. PMID: 32210163; PMCID: PMC7151639.
22. Trott O, Olson AJ. AutoDock Vina: improving the speed and accuracy of docking with a new scoring function, efficient optimization, and multithreading. J Comput Chem. 2010 Jan 30;31(2):455-61. doi: 10.1002/jcc.21334. PMID: 19499576; PMCID: PMC3041641.
23. Van Der Spoel D, Lindahl E, Hess B, Groenhof G, Mark AE, Berendsen HJ. GROMACS: fast, flexible, and free. J Comput Chem. 2005 Dec;26(16):1701-18. doi: 10.1002/jcc.20291. PMID: 16211538.

24. Vanommeslaeghe, K. Hatcher, E. Acharya, C. Kundu, S. Zhong, S. Shim, J. E. Darian, E. Guvench, O. Lopes, P. Vorobyov, me. and MacKerell, Jr. A.D. "CHARMM General Force Field (CGenFF): A force field for drug-like molecules compatible wif the CHARMM all-atom additive biological force fields," Journal of Computational Chemistry 31: 671-90, 2010, PMC2888302 [DOI]
25. Vlaming M, Bilemjian V, Freile JÁ, Melo V, Plat A, Huls G, Nijman HW, de Bruyn M, Bremer E. Tumor infiltrating CD8/CD103/TIM-3-expressing lymphocytes in epithelial ovarian cancer co-express CXCL13 and associate with improved survival. Front Immunol. 2022 Oct 21;13:1031746. doi: 10.3389/fimmu.2022.1031746. PMID: 36341460; PMCID: PMC9633842.
26. Wu M, Wu A, Zhang X, Li Y, Li B, Jin S, Dong Q, Niu X, Zhang L, Zhou X, Du J, Wu Y, Zhai W, Zhou X, Qiu L, Gao Y, Zhao W. Identification of a novel small-molecule inhibitor targeting TIM-3 for cancer immunotherapy. BiochemPharmacol. 2023 Jun;212:115583. doi: 10.1016/j.bcp.2023.115583. Epub 2023 May 4. PMID: 37148978.
27. Yu WD, Sun G, Li J, Xu J, Wang X. Mechanisms and therapeutic potentials of cancer immunotherapy in combination with radiotherapy and/or chemotherapy. Cancer Lett. 2019 Jun 28;452:66-70. doi: 10.1016/j.canlet.2019.02.048. Epub 2019 Mar 19. PMID: 30902563.
28. Zhang Y, Cai P, Li L, Shi L, Chang P, Liang T, Yang Q, Liu Y, Wang L, Hu L. Co-expression of TIM-3 and CEACAM1 promotes T cell exhaustion in colorectal cancer patients. Int Immunopharmacol. 2017 Feb;43:210-218. doi: 10.1016/j.intimp.2016.12.024. Epub 2016 Dec 28. PMID: 28038383.

UNDER PEER REVIEW